Eur. Phys. J. B **26**, 199–209 (2002)
DOI: 10.1140/epjb/e20020081

THE EUROPEAN PHYSICAL JOURNAL B
EDP Sciences

Competing polarization mechanisms in the heavy-fermion paramagnet $CeCu_6$

Site specific NMR information for $CeCu_6$ powder samples

M. Winkelmann, G. Fischer, B. Pilawa, and E. Dormann[a]

Physikalisches Institut, Universität Karlsruhe, Wolfgang-Gaede-Str. 1, 76128 Karlsruhe, Germany

Received 20 November 2001

Abstract. Nuclear magnetic resonance (NMR) and relaxation of ^{63}Cu and ^{65}Cu in a powder sample of the heavy-fermion paramagnet $CeCu_6$ is measured and analysed quantitatively. Five different Cu sites are accessible to a detailed analysis. We derive quadrupolar splitting frequencies, Ce to Cu transferred hyperfine field coupling constants, and transversal as well as longitudinal relaxation behaviour. Only small relaxation anomalies are observed at the orthorhombic to monoclinic structural phase transition of $CeCu_6$. We point to the different importance of transferred hyperfine interaction and local conduction electron density for static or dynamic part, respectively, of Cu hyperfine interaction. The different sign of the transferred hyperfine interaction from Ce^{3+} to different Cu neighbours reveals the different competing interaction mechanisms, giving rise to the heavy-fermion paramagnetic behavior of $CeCu_6$.

PACS. 76.60.-k Nuclear magnetic resonance and relaxation – 75.20.Hr Local moment in compounds and alloys; Kondo effect, valence fluctuations, heavy fermions

1 Introduction

The pseudo-binary intermetallic compounds $CeCu_{6-x}Au_x$ ($0 \leq x \leq 1$) received considerable interest in recent years [1]. $CeCu_6$ is one of the best-known heavy-fermion systems that orders magnetically not above 2 mK [2–4]. On the other hand, the isoelectronic ternary, structurally ordered compound $CeCu_5Au$ orders antiferromagnetically at $T_N = 2.3$ K, already [5]. For pseudo-binary compounds $CeCu_{6-x}Au_x$ with $x \approx 0.1$, at the magnetic-nonmagnetic boundary for $T_N \to 0$, signatures of non-Fermi liquid behaviour were found [6].

The main difficulty that prevented up to now a detailed local-probe analysis of the x-dependence of the interplay between long-distance antiferromagnetic RKKY-like coupling of the Ce^{3+} moments [7,8] and Kondo-like shielding of the individual Ce^{3+} moments, arises from the relatively complicated crystal structure with four formula units per unit cell [9]. The reduced symmetry of the cerium sites (4(c)) allows that the local preferred magnetic axes of the Ce^{3+} ions deviate by unknown angles of plus and minus $\theta_0(x)$ from the magnetically "easy" c-axis, yet being restricted to the a-c plane of $CeCu_{6-x}Au_x$. There is a monoclinic distortion ($P2_1/c$) of the orthorhombic room temperature crystallographic structure (Pnma) of $CeCu_6$ occurring at about 230 K [10,11]. The eight Cu(1) sites of the orthorhombic structure, being the only atoms not restricted to the 1/4 b and 3/4 b planes of $CeCu_6$, shift at the orthorhombic to monoclinic phase transition and split into inequivalent four Cu(1) and four Cu(6) sites [9,11]. In accordance with these structural characteristics, six NQR frequencies were derived at low temperature [20] (Tab. 1).

We want to point here to a structural peculiarity of $CeCu_6$. The average Ce-Cu distance of $CeCu_6$, $d = 3.146$ Å [9], is clearly above the sum of the tabulated element radii $r_{Ce} = 1.82$ Å and $r_{Cu} = 1.27$ Å, *i.e.* $r_{Ce} + r_{Cu} = 3.09$ Å [30]. There are two sites, Cu(4) and Cu(5), however, which have a clearly smaller average separation of 2.95 Å, only (Tab. 1). These Cu(4) and Cu(5) sites are squeezed between subsequent Ce sites along the b direction in a 120°-zigzag like Ce-Cu(4)-Ce as well as Ce-Cu(5)-Ce rhombic chain arrangement. The respective third Ce^{3+} nearest neighbour is situated on the Cu(4) and Cu(5) atom's own $a-c$ plane, shifted in a direction, but at rather close c-axis coordinates. For these sites, anomalies of the transferred hyperfine interaction should therefore be expected, caused by covalency and wave-function overlap effects. The magnetic hyperfine interaction of the Cu sites is studied here for the first time by a locally sensitive method as is NMR.

The large number of inequivalent Cu sites opens in principle the possibility to monitor independently the conduction electron polarization at several positions in the unit cell *via* nuclear magnetic resonance (NMR) of the two Cu isotopes ^{63}Cu and ^{65}Cu (Tab. 2). The almost Ising-like anisotropy of the 4f-electronic low-temperature

[a] e-mail: edo@piobelix.physik.uni-karlsruhe.de

Table 1. Site specific information for Cu sites in $CeCu_6$. Numbering and values of the quadrupole frequencies of the ^{63}Cu-NQR in $CeCu_6$ [20] are given in the upper block. Nearest Ce neighbour number N_{Ce}, average distance $\bar{d}_{Ce}$ and transferred dipolar fields and RKKY-sum calculated from the orthorhombic structural data [9] ($r_{max} = 800$ Å) are compiled in the lower block (see text). The association of structural sites and NQR lines, proposed in [20], is used when arranging both data sets, but questioned below.

^{63}Cu-NQR line	O	I	II	III	IV	V	[20]
^{63}Cu-NQR frequency/MHz	0.45	3.90	6.13	6.80	10.2	11.3	[20]

structural site	Cu(5)	Cu(3)	Cu(4)	Cu(1)	Cu(2)	Cu(6)	[9,20]
N_{Ce}	3	3	3	3	4	3	[9]
$\bar{d}_{Ce}$/Å	2.948	3.236	2.951	3.207	3.283	3.207	[9]
$\alpha_a^{dip}/\mathrm{kOe}\mu_B^{-1}$	+0.258	−0.531	+0.126	+0.039	−0.067	+0.039	
$\alpha_b^{dip}/\mathrm{kOe}\mu_B^{-1}$	+0.522	+0.071	+0.447	−0.331	−0.229	−0.331	
$\alpha_c^{dip}/\mathrm{kOe}\mu_B^{-1}$	−0.779	+0.460	−0.573	+0.291	+0.296	+0.291	
α_{RKKY}/rel. units	-2.4×10^{-3}	-3.7×10^{-3}	-2.5×10^{-3}	-2.1×10^{-3}	-5.9×10^{-3}	-2.1×10^{-3}	

Table 2. NMR data used in the current analysis [8,12,13].

Isotope	^{63}Cu	^{65}Cu	ratio 63/65
abundancy	69.1 %	30.9 %	2.24
I	3/2	3/2	
$\gamma/_2\pi$ / MHz/T	11.285	12.090	0.933
$Q/\ 10^{-24}\mathrm{cm}^2$	−0.211	−0.195	1.08

magnetization [14–18] and the low Cu-site symmetry causes fully developed anisotropy of electric quadrupolar and magnetic dipolar interactions for the two Cu isotopes, however. This prevented a detailed study of locally resolved single crystal NMR anisotropies in external magnetic field up to now. Nevertheless, in the high-temperature range (140–470 K), from a linear correlation of the Cu-NMR line Knight shift and the magnetic susceptibility of $CeCu_6$ [32,33], $J_{sf} = -0.012$ eV was derived within the uniform polarization model [8], equivalent to a coupling constant for the transferred field from Ce^{3+} to Cu nuclei of $\overline{\alpha} = +0.5\,\mathrm{kOe}/\mu_B$ (for $K_0 = +0.3\%$). NMR relaxation in external magnetic field was studied using the powder averaged $+1/2 \leftrightarrow -1/2$ transitions only [19]. The much larger width of the spin echo powder spectrum of ^{63}Cu and ^{65}Cu in $CeCu_6$, compared to isostructural $LaCu_6$, was reported as indication that only Ce causes the very strong anisotropic hyperfine interaction [19]. A detailed NQR analysis of the $\pm1/2 \leftrightarrow \pm3/2$ transitions gave the main values of the quadrupolar splittings [20], the respective relaxation rates of some of these NQR lines [20–22], and was used to correlate structural sites and quadrupolar splitting parameters [20], as is used for arranging Table 1. Yet, this assignement of the structural sites and NQR lines must be considered as tentative [20], because it relies on the proportionality of the actual electric field gradients and the results of point charge model calculations, considering Ce^{3+} charges alone. NQR can neither determine the local conduction electron contact densities (*i.e.*, Knight shift), nor the conduction electron exchange polarization by the $4f$ ion for a paramagnet (*i.e.*, paramagnetic NMR line shifts), however. Thus it is not appropriate in order to unravel the electronic structure of a paramagnetic heavy-fermion compound.

Recently, we showed that the NMR spectra of powdered $CeCu_5Au$ single crystals in external magnetic field can be substantially simplified, if the powder sample is oriented at low temperature by means of its large magnetic anisotropy [23]. The Cu-site with 3.9 MHz main value of the ^{63}Cu quadrupolar splitting (NQR-frequency I, abbreviated as Cu[I] in the following) could thus be analysed separately, the signal in the earlier NQR analysis being supposed to originate from ^{63,65}Cu at the 4(c) sites numbered Cu(3) [9,20]. The anisotropy of quadrupolar interaction, transversal and longitudinal relaxation have been observed. Most importantly, the coupling constant α of the transferred magnetic hyperfine interaction from all Ce moments to this site (see Eq. (2) below for definition) was unravelled, varying only weakly with orientation from $\alpha_{\|c} = +(1.26 \pm 0.12)\,\mathrm{kOe}/\mu_B$ to $\alpha_{\|a} = +(1.21 \pm 0.12)\,\mathrm{kOe}/\mu_B$ [24]. The transferred field coupling constant $\alpha_i(n)$ for Cu site n is composed of two contributions,

$$\alpha_i(n) = \alpha_i^{\mathrm{dip}}(n) + \alpha_i^{\mathrm{RKKY}}(n), \qquad (1)$$

i.e., the classical dipolar field coupling constant $\alpha_i^{\mathrm{dip}}(n)$ and the real transferred hyperfine field contribution, $\alpha_i^{\mathrm{RKKY}}(n)$. α_i^{dip} can be calculated from the known crystal structure and is caused by the total $4f$ electronic moment, *i.e.* spin and orbital moments. The in-field components for $CeCu_6$ are reported in Table 1, for the three main axes of the orthorhombic high-temperature structure. For the Cu(3), Cu(4) and Cu(5) sites, the classical dipolar field causes the anisotropy of the coupling constant α to be larger than $1\,\mathrm{kOe}/\mu_B$. On the other hand, the non-classical part α_i^{RKKY} results from fermi-contact interaction of the Cu *s*-like conduction electrons with the ^{63,65}Cu nucleus after exchange polarization through the Ce^{3+} electron spin (see Eq. (3) below). The latter amounts to $S = 1/2$, only, for the Ce^{3+} Hund's rule ground state $^2F_{5/2}$, to be compared with the total angular

moment $J = 5/2\,(L = 3, g_J = 6/7)$ or more precisely, it is reduced by $(g_J - 1)/g_J = -1/6$. Thus both contributions in equation (1) may well be of comparable importance in $CeCu_{6-x}Au_x$. We concluded in [23], that, whereas the total field transferred from the Ce^{3+} moments to the Cu[I] sites is highly anisotropic in $CeCu_5Au$, varying by a factor of 5 between c and a direction, this anisotropy is primarily caused by the Ising-like anisotropy of the Ce^{3+} low-temperature moment, and only to a minor part by the anisotropy of the coupling constant α_i[I]. It should be mentioned, that the observed small anisotropy $\alpha_{\|c} - \alpha_{\|a} = +(0.05 \pm 0.24)\mathrm{kOe}/\mu_\mathrm{B}$ for the Cu[I] lines in $CeCu_5Au$ disagrees with the expected dipolar anisotropy of the Cu(3) site (Tab. 1), but points to an assignment to the Cu(1/6) sites instead, thus questioning the assignment of [20].

In the current analysis, we extend this type of NMR study to an oriented powder sample of $CeCu_6$, with the difference that a polycrystalline bulk sample was used for the preparation of the powder sample [25]. We show that five different Cu-sites can, nevertheless, be distinguished by NMR, using the known main values of quadrupolar splittings for discrimination. Anisotropy of quadrupolar splitting and central line longitudinal and transversal relaxation are derived. Most importantly, the transferred hyperfine field coupling constants $\alpha_i(n)$ are determined and Cu sites with – compared to the $CeCu_5Au$ analysis of the Cu[I] line or the earlier average value for $CeCu_6$ [32,33] – opposite sign and largely enhanced value of the transferred hyperfine interaction α are observed for $CeCu_6$. Based on our analysis, we argue that Cu nuclear spin-lattice relaxation reflects in $CeCu_6$ for temperatures above 10 K primarily the local conduction electron spin density and character at the respective lattice site. The fluctuating transferred magnetic hyperfine fields, that bring about the influence of the Ce^{3+} spin dynamics on nuclear spin relaxation, seem to gain in importance only for even lower temperatures, when the spin-dynamics of the electronic moments are slowed-down in the $CeCu_6$ paramagnet (in contrast to $CeCu_5Au$, that orders at $T_N = 2.3$ K already). The static part of the transferred hyperfine interaction reveals clearly that a simplyfied RKKY model fails to explain the different signs found for the transferred hyperfine couplings at various Cu sites in this prototype of a heavy fermion paramagnet.

2 Experimental details

A powdered polycrystalline $CeCu_6$ sample was sealed in a quartz glas tube (ca. 0.5 g, 20–50 μm grain size). Due to the Ising-like low-temperature magnetic anisotropy of $CeCu_6$, single crystalline grains can be oriented in external applied magnetic field. The degree of preferential grain orientation depends on sample history. It can be improved by starting 7 T-measurements at the lowest temperature (4 K) instead of the highest one. But concluding from the experimental results, a large part of the individual grains of our powder sample must be polycrystalline,

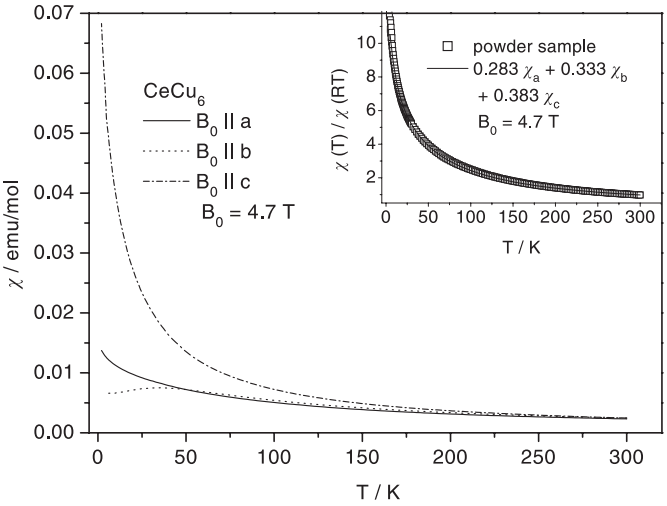

Fig. 1. Magnetic susceptibility of a $CeCu_6$ single crystal for external magnetic field ($B_0 = 4.7$ T) along the crystallographic main axes (orthorhombic denotation). The inset shows the susceptibility χ of the NMR powder sample, normalized to room temperature, together with the fitted mixture of the main axis values, $0.283\,\chi_a + 0.333\,\chi_b + 0.383\,\chi_c$.

thus preventing their uniform alignment in external magnetic field. According to SQUID magnetometer analysis, the powder grains are oriented only slightly in favour of the most magnetic c direction at $B_0 = 4.7$ T (Fig. 1, orthorhombic denotation). Variable frequency NMR spectra were recorded at fixed field (7 T) with a Bruker MSL 300 spectrometer. Variable field of an electromagnet (<1.9 T) and a Bruker CXP 200 spectrometer were used for low-frequency measurements. Home-built probe heads and an Oxford Instruments variable temperature cryostat were employed in both magnets. For details of the NMR techniques adopted we refer to [23,26]. For the sake of clarity we have to point to the fact that the spectra shown in Figures 2 and 3 are not corrected for spin-echo decay proportional to $\exp(-2\tau/T_2(\nu))$ or frequency dependence of excitation conditions (*e.g.* the difference between central lines and quadrupolar satellites). It is also important to note that the NMR signal in Figure 2 is non-zero everywhere between 75 MHz and 90 MHz, that means also between the prominent peaks, and that we currently do not yet really understand, why a polycrystalline powder sample gives such well resolved NMR spectra.

3 Experimental results

Figure 2 shows the NMR spin echo Fourier transform spectrum of the $CeCu_6$ powder sample recorded at $B_0 = 7$ T as function of frequency at $T = 20$ K. For further reference, the most prominent NMR lines are numbered and assigned. The central lines ($+1/2 \leftrightarrow -1/2$ transitions, index z in the following) for ^{63}Cu around about 79.55 MHz and for ^{65}Cu at about 85.22 MHz (Figs. 2 and 3) can be distinguished from the quadrupole satellites (index R, L in the following). After a detailed field-, frequency- and

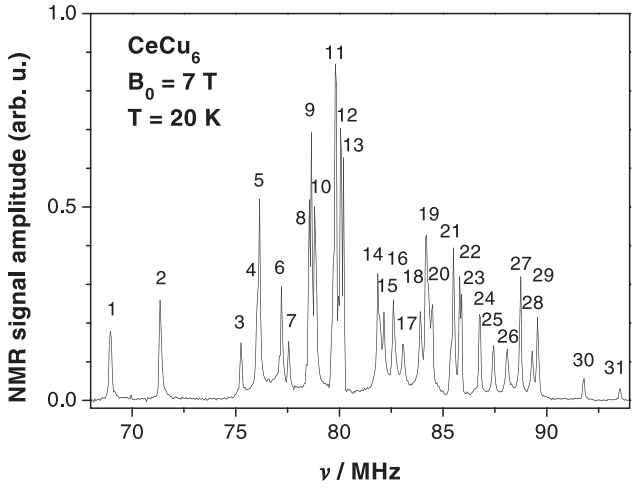

Fig. 2. Uncalibrated NMR spin-echo Fourier transform spectrum of $CeCu_6$ powder sample *versus* frequency ($B_0 = 7\,\mathrm{T}$, $T = 20\,\mathrm{K}$) excited with two pulses of $2\,\mu\mathrm{s}$ and $4\,\mu\mathrm{s}$ duration and $50\,\mu\mathrm{s}$ separation. (The sensitivity of the probehead decreases for frequencies above 90 MHz). The NMR lines, numbered for further reference, are assigned to: 1: $^{63}\underline{\mathrm{A}}_L$, 2:$^{63}\underline{\mathrm{B}}_L$, 3: $^{65}\underline{\mathrm{A}}_L$, 4: $^{63}\mathrm{C}_L$, 5: $^{63}\mathrm{D}_L$, 6: $^{63}\underline{\mathrm{C}}_L$, 7: $^{63}\underline{\mathrm{A}}_z$, 8: $^{65}\underline{\mathrm{B}}_L$, 9: $^{63}\underline{\mathrm{E}}_L/^{63}\underline{\mathrm{E}}_z$, 10: $^{63}\underline{\mathrm{E}}_z/^{63}\underline{\mathrm{E}}_R$, 11: $^{63}\underline{\mathrm{B}}_z/^{63}\underline{\mathrm{C}}_z/^{63}\underline{\mathrm{D}}_z$, 12: $^{63}\mathrm{C}_z$, 13: $^{63}\mathrm{D}_z$, 14: $^{65}\mathrm{C}_L$, 15: $^{65}\mathrm{D}_L$, 16: $^{63}\underline{\mathrm{C}}_R$, 17: $^{65}\underline{\mathrm{C}}_L/^{65}\underline{\mathrm{A}}_z$, 18: $^{63}\mathrm{D}_R$, 19: $^{63}\mathrm{C}_R$, 20: $^{65}\underline{\mathrm{E}}_z$, 21: $^{65}\underline{\mathrm{B}}_z$, 22: $^{65}\underline{\mathrm{C}}_z/^{65}\underline{\mathrm{D}}_z$, 23: $^{65}\mathrm{C}_z/^{65}\mathrm{D}_z$, 24: $^{63}\underline{\mathrm{A}}_R$, 25: $^{63}\underline{\mathrm{B}}_R$, 26: $^{65}\underline{\mathrm{C}}_R$, 27: $\underline{\mathrm{F}}_R$, 28: $^{65}\mathrm{D}_R$, 29: $^{65}\mathrm{C}_R$, 30: $^{65}\underline{\mathrm{A}}_R$, 31: $^{65}\underline{\mathrm{B}}_R$. For further analysis, the average of 9+10 was used as $^{63}\underline{\mathrm{E}}_z$.

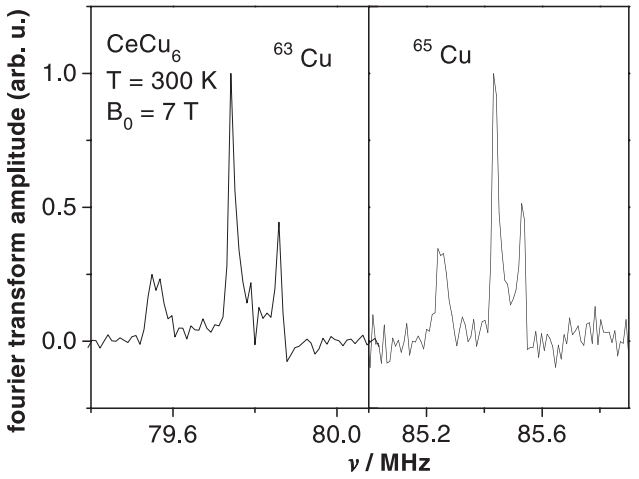

Fig. 3. NMR spin-echo Fourier transform spectrum of weakly oriented $CeCu_6$ powder sample excited with two pulses of $2\,\mu\mathrm{s}$ and $4\,\mu\mathrm{s}$ duration and $50\,\mu\mathrm{s}$ separation. $B_0 = 7\,\mathrm{T}$, $T = 300\,\mathrm{K}$, $\nu_{rf} = 79.8\,\mathrm{MHz}$ (85.5 MHz) for ^{63}Cu (^{65}Cu). $\nu_{0,z} = 79.55\,\mathrm{MHz}$ (85.22 MHz). The details of the 300 K-spectrum depend on sample measurement history (degree of grain orientation).

temperature-dependent analysis, most satellites could be identified. For varied temperature they shift by several MHz and even intersect due to the different sign of their paramagnetic shifts. The three-line spectra originating from Cu nuclei with the external magnetic field parallel to the main axis of their local electric field gradient (generally denoted $\vartheta = 0$) could easily be identified *via* their approx-

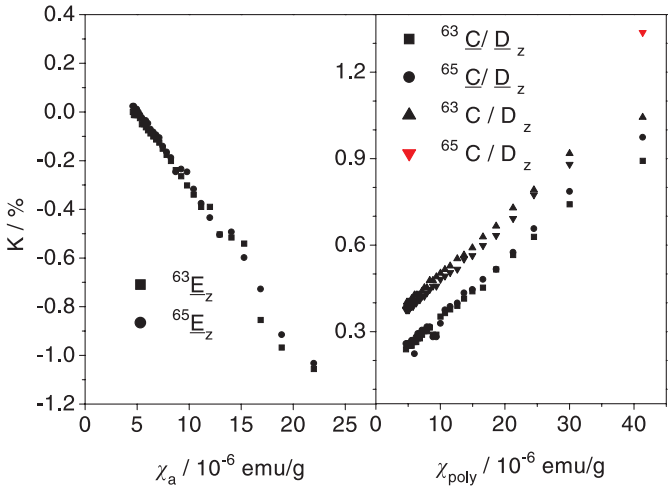

Fig. 4. Temperature dependence of the central line positions for both Cu isotopes ^{63}Cu, and ^{65}Cu in the $CeCu_6$ powder sample at $B_0 = 7\,\mathrm{T}$, given as Jaccarino-Clogston plots $K(T)$ *versus* $\chi(T)$, with T as an implicit parameter. Due to the overlap of the central NMR lines, also the symbols marked C/D$_z$ represent an orientational average.

imate equidistance and a separation corresponding to the known NQR data (Tab. 1). The other three-line spectra thus originate from field directions not parallel to a main axis ($\vartheta \neq 0$). The respective direction of the electrical field gradient's main axis was not deduced *via* model calculation of the local field gradient, however. The identified lines are nominated according to "site" (A, B, ..., F), high or low-frequency quadrupolar satellite (R, L), or Zeeman line (Z), isotope ^{63}Cu or ^{65}Cu and main (A, B, ..., F) or not main axis (A, B, ...) of the field gradient, *e.g.* $^{63}\underline{\mathrm{A}}_L$, for the low-frequency not-main axis satellite of ^{63}Cu at the site called "A". The quadrupole parameters thus derived are collected in Table 3. The quadrupolar splitting for the "site E" was of the order of 0.3 MHz and below for the orientations observed with our powder sample and could not reliably be analyzed. The temperature dependence of the central line peak positions is plotted in Figure 4 *versus* magnetic susceptibility with T as implicit parameter. At room temperature all the central resonance frequencies were found above the pure Zeeman frequencies 79.55 MHz and 85.22 MHz of ^{63}Cu and ^{65}Cu, respectively, in the superconducting magnet's field, *i.e.* 79.56 MHz, 79.74 MHz and 79.86 MHz or 85.25 MHz, 85.43 MHz and 85.53 MHz, respectively (Fig. 3). The upper two lines shift to higher frequency, the lower one to lower frequency, with the equivalent behaviour for both isotopes (Fig. 4). Paramagnetic shifts were also determined for several quadrupolar satellites (Fig. 5).

Line separation for the central lines is not complete. Nevertheless, derivation of individual transversal and longitudinal relaxation rates for the six central line positions was attempted. Figure 6 collects the T_2 data. In Figure 7, the T_1 data recorded for the three central lines of both isotopes are shown separately, together with their ratio $R_{21} = {}^{65}T_1^{-1}/{}^{63}T_1^{-1}$. In addition, spin-lattice relaxation rates were derived for selected quadrupole satellites.

Table 3. Quadrupole parameters derived from NMR spectra of $CeCu_6$ powder sample ($T = 20\,\mathrm{K}$). For denominations see text and caption of Figure 2.

NMR lines	$^{63}\nu_Q$/MHz	$^{65}\nu_Q$/MHz	ratio 63/65	NQR line [20]	η
$^{63}\underline{A}$, $^{65}\underline{A}$	8.93 ± 0.28	8.25 ± 0.45	1.082	V/IV	0.58/0.75
$^{63}\underline{B}$, $^{65}\underline{B}$	8.03 ± 0.58	7.49 ± 0.69	1.072	IV/V	0.57/0.42
^{63}C, ^{65}C	4.07 ± 0.02	3.83 ± 0.05	1.063	I/?	
^{63}D, ^{65}D	3.89 ± 0.19	3.55 ± 0.03	1.095	I/?	
$^{63}\underline{C}/^{63}\underline{D}$, $^{65}\underline{C}/^{65}\underline{D}$	2.70 ± 0.10	2.50 ± 0.05	1.08	I/?	$\underline{C}$) 0.32 ± 0.01/$\underline{D}$) 0.40 ± 0.01

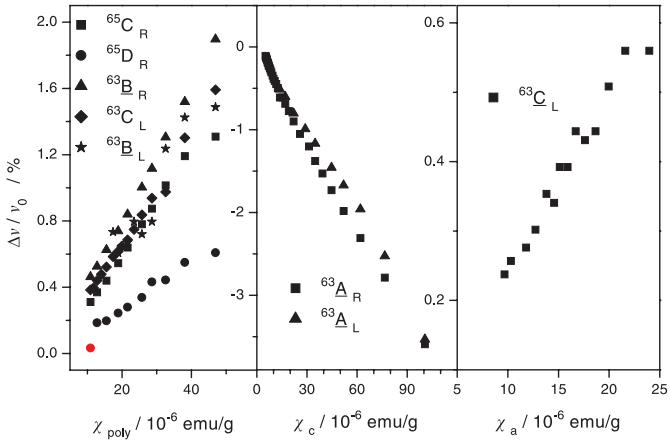

Fig. 5. Jaccarino-Clogston plots for selected quadrupole satellite line shifts of ^{63}Cu and ^{65}Cu for $CeCu_6$ powder sample at $B_0 = 7\,\mathrm{T}$. Using the temperature as an implicit parameter, $\Delta\nu(T)/\nu_{0,z}$ is plotted *versus* the appropriate combination of single crystal magnetic susceptibilities $\chi(T)$.

4 Analysis

At temperatures above 50 K, the difference between *a*- and *b*-axis magnetic susceptibility (Fig. 1) is too small to allow the discrimination of these two axes for the total powder magnetic susceptibility. The data measured for $B_0 = 4.7\,\mathrm{T}$ at temperatures below 20 K (Fig. 1, inset) indicate that all crystalline orientations appear with almost equal probability, exhibiting only a slight preference of orienting the most magnetic *c*-axis parallel to the field direction. This points to the polycrystallinity even of the individual powder grains used for the current NMR analysis.

The correlation of the central and satellite NMR line shifts with the single crystal magnetic susceptibility (Sect. 4.2 and Figs. 4, 5) reveals more clearly that some of the NMR lines correspond exclusively to magnetic field orientations in the *c*-*a* plane (orthorhombic denotation). Therefore, at most two main values of the quadrupole splitting and transferred hyperfine interaction parameters are accessible by the current NMR analysis.

4.1 Quadrupole splitting parameters

Analysis of the NMR spectra along the lines reported for $CeCu_5Au$ [23], using the standard relations [27,28] yields the values tabulated in Table 3. A larger number of sites

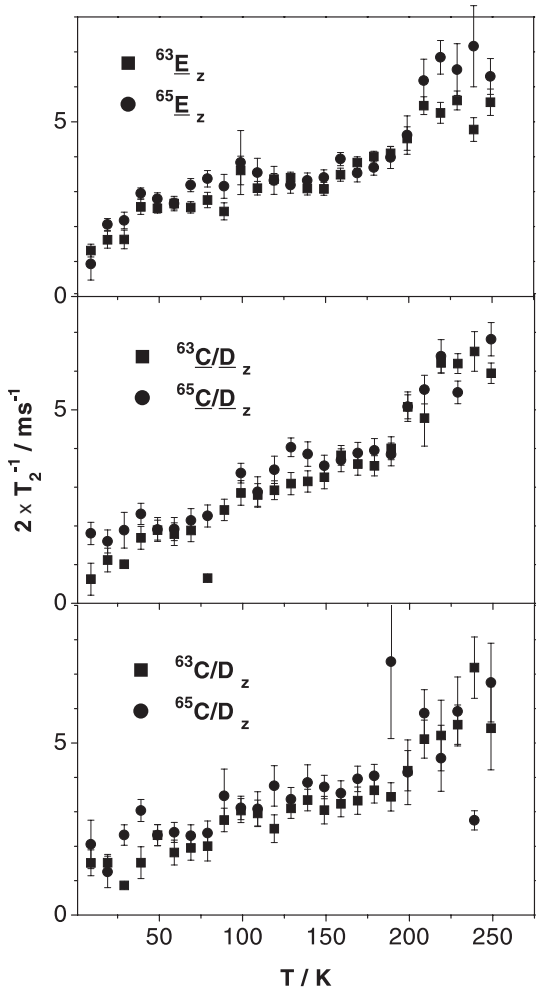

Fig. 6. Spin echo decay constant, T_2^{-1}, *versus* temperature for the three central lines of both Cu isotopes in $CeCu_6$ powder sample ($B_0 = 7\,\mathrm{T}$). The orthorhombic to monoclinic phase transition occurs at about 200 K. For the denotation of the NMR lines see also Figure 4. The temperature dependence can be approximated by a straight line $r_0 + r_1 \cdot T$. (Tab. 5).

than in $CeCu_5Au$ is observed, with the numbering of NQR lines of reference [20] given for comparison. This association is in most cases not unique, leading to a choice of asymmetry parameters η as well. The identified quadrupolar satellites ($\pm 1/2 \leftrightarrow \pm 3/2$ transitions) and second order shifted Zeeman lines ($+1/2 \leftrightarrow -1/2$ transitions) are indicated in the caption to Figure 2. Only one line (27, $\underline{F}_R$)

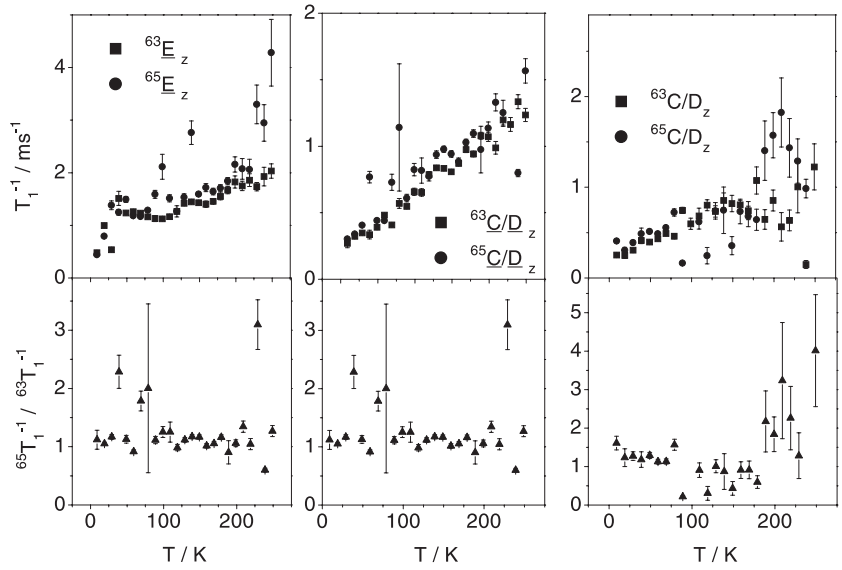

Fig. 7. Spin-lattice relaxation rates of the two Cu isotopes ^{63}Cu and ^{65}Cu for the three central lines $\underline{\mathrm{E}}_z$, $\underline{\mathrm{C}}_z/\underline{\mathrm{D}}_z$ and $\mathrm{C}_z/\mathrm{D}_z$. The ratio $R_{21} = {}^{65}T_1^{-1}/{}^{63}T_1^{-1}$ is plotted in the lower part. For the denotation of the NMR lines see also Figure 4. Again, the rates were parameterized as $r_0 + r_1 \cdot T$. (Tab. 5) (differences of the T_1-scales have to be considered).

Table 4. Transferred field coupling parameters derived from Jaccarino-Clogston plot for $CeCu_6$. For derivation and definitions, see text and caption of Figure 2 and Figure 4. "poly" means that $\chi(T) = 0.283\,\chi_a + 0.333\,\chi_b + 0.383\,\chi_c$ was used for $\mathrm{d}K/\mathrm{d}\chi$ from the inset to Figure 1. Orthorhombic denotation is used in account of the smallness of the monoclinic distortion. Assignment to isotope ^{63}Cu or ^{65}Cu for $\underline{\mathrm{F}}_R$ line is unclear ($\pm$10% error bar). NQR-line assignment according to [20].

NMR-lines	orientation	α/kOeμ_B^{-1}	NQR-line [20]
$^{63}\underline{\mathrm{A}}_L$, $^{63}\underline{\mathrm{A}}_R$	c	-3.78 ± 0.18	V/IV
$^{63}\underline{\mathrm{B}}_L$, $^{63}\underline{\mathrm{B}}_R$	poly	$+3.90 \pm 0.17$	IV/V
$^{63}\mathrm{C}_z/^{63}\mathrm{D}_z$, $^{65}\mathrm{C}_z/^{65}\mathrm{D}_z$	poly	$+2.64 \pm 0.54$	I/?
$^{63}\mathrm{C}_L$, $^{65}\mathrm{C}_R$	poly	$+ 3.35 \pm 0.17$	I/?
$^{65}\mathrm{D}_R$	poly	$+ 1.46 \pm 0.15$	I/?
$^{63}\underline{\mathrm{C}}_z/^{63}\underline{\mathrm{D}}_z$, $^{65}\underline{\mathrm{C}}_z/^{65}\underline{\mathrm{D}}_z$	poly	$+1.63 \pm 0.47$	I/?
$^{63}\underline{\mathrm{C}}_L$	a	$+2.68 \pm 0.27$	I/?
$^{63}\underline{\mathrm{E}}_z$, $^{65}\underline{\mathrm{E}}_z$	a	-6.68 ± 0.04	0
$^{63/65}\underline{\mathrm{F}}_R$	c	$-4.34/-4.05$	?

is left unexplained, because the respective partner lines probably overlap with assigned lines and because this line has a very strong paramagnetic shift (Tab. 4).

4.2 Central and satellite line paramagnetic shifts

Recently we showed that the almost Ising-like anisotropy of the magnetic susceptibility of $CeCu_{6-x}Au_x$ intermetallic compounds allows the determination of single-crystal powder grain orientation in external magnetic fields with help of the well-known Jaccarino-Clogston plot [23,8]. This analysis is not at all trivial, for the current powder sample of $CeCu_6$, because the low symmetry of the four Ce and the – in each case four – Cu(1) to Cu(6) sites does not fix the $^{63/65}$Cu local electric field gradient direction or the individual Ce^{3+} moment's Ising axis to the a, b, c directions of the unit cell. Fortunately, however, the relative temperature dependence of the total magnetic susceptibility for a single crystal oriented with external field along different ones of these three crystallographic axes differs so drastically for temperatures below 50 K (Fig. 1), that it is possible to correlate unequivocally the temperature dependence of the paramagnetic shift of an individual Cu NMR line, observed for an at first unknown orientation of the respective powder grain and local Cu electric and magnetic hyperfine interaction tensor, with the respective combination of the magnetic susceptibility's main values. If the observed NMR line results from a superposition of the signals of grains with a distribution of orientations instead of being due to a well defined orientation of the elementary cell with respect to the external field, this

correlation is still possible, but can not yield more than a poorly defined average of the respective hyperfine coupling constants. The linearity of this K *versus* χ plot, with temperature T as an implicit parameter, and with $\chi = p_a\chi_a + p_b\chi_b + p_c\chi_c$, is thus the criterion for the derivation of the orientational parameters p_a, p_b, p_c. Figure 4 shows the best fits obtained for the central lines discerned in Figures 2 and 3 by combining the χ_a, χ_b, χ_c-data of Figure 1. The coupling constants α

$$K(T) = \frac{\Delta\nu}{\nu_0} = K_0 + \alpha\chi_{\rm mol}(T)/N_A \qquad (2)$$

together with the orientational information are collected in Table 4. According to our analysis, the two lines at 79.74 MHz, 79.86 MHz or 85.43 MHz, 85.53 MHz in Figure 3 correspond to the powder-distribution edge singularities (*i.e.*, $\cos^2\theta \approx 0$ and $\cos^2\theta \approx 5/9$) of the $+1/2 \leftrightarrow -1/2$ transition of NQR-line I, analysed already for $CeCu_5Au$ [23]. It is evident, that most Zeeman-line coupling constants in Table 4 present an ill-defined orientational average. Fortunately, the temperature dependent line shift could also be analysed for several quadrupole satellites (Fig. 5, index R, L in Tab. 4). The coupling constant thus derived for the D-line is small and positive like was observed for the Cu[I] lines in $CeCu_5Au$. Thus one might be tempted to conclude that only the D-lines correspond to the Cu[I] NQR line of $CeCu_{6-x}Au_x$. The C-lines have a considerably larger coupling constant α ranging between +2.6 and +3.4 kOe/μ_B. In this respect it was important to follow the temperature dependence of the C- and D-line quadrupolar satellites *versus* temperature in the temperature range of the orthorhombic to monoclinic phase transition. Whereas the C-line could easily be followed from 10 K to room temperature (as observed for the central Cu[I] signal in $CeCu_5Au$) the D-line was lost below 180 K, already. On the other hand, the coupling constant of the central line $\underline{E}_z$ is the largest one and of opposite sign. It originates only from grains with magnetic field parallel to their a-axis and from the Cu site yielding 0.45 MHz quadrupolar splitting (NQR-line Cu[0] according to [20]). Obviously, not the main value of quadrupole splitting, but a perpendicular principal value is observed here. We want to emphasize that the coupling constants α compiled in Table 4 are in part more than a factor of 10 larger than the average value $\overline{\alpha} = +0.5$ kOe/μ_B derived in the early high-temperature analysis [32,33] and, obviously, they differ even in sign. Interestingly, also the bare Knight shifts of the sites are different and amount to K_0(C,$\underline{\rm C}$/D,$\underline{\rm D}$) = $+(0.22 \pm 0.07)\%$ and $K_0(\underline{\rm E}) = +(0.315 \pm 0.007)\%$.

4.3 Central and satellite line relaxation rates

Except for the early NMR investigations of $CeCu_6$ powder samples [19], most relaxation studies of $CeCu_6$ analysed selected $\pm 1/2 \leftrightarrow \pm 3/2$ transitions of NQR spectra [21,22,29]. Due to the similarity of the quadrupole moments of both Cu isotopes (Tab. 2), their NQR signals overlap partially [20,21]. Therefore, anomalies in the temperature dependence of transversal relaxation rates are frequently observed [20]. No relevant variation of spin-spin relaxation rates for the three central lines of our $CeCu_6$ powder sample is seen in Figure 6. The Korringa-like linear slopes (r_1) of $1/T_2$ are given in Table 5. Their ratio for both isotopes compares reasonably with the ratio of the square of their gyromagnetic ratios. The extrapolated zero-temperature $1/T_2$ rates (r_0) amount to 0.9 – 0.95 ms^{-1} for the $\underline{\rm E}_z$ lines and 0.5 – 0.65 ms^{-1} for the $\underline{\rm C}_z/\underline{\rm D}_z$ and $\rm C_z/D_z$ lines. Small anomalies of the $1/T_2$ rates are seen in the temperature range (200–230 K) of the orthorhombic to monoclinic phase transition (Fig. 6). Due to the better line separation compared to our earlier measurements at $B_0 = 4.7$ T, the spin lattice relaxation rates derived for the three central lines at $B_0 = 7$ T, shown in Figure 7, are less noisy than our earlier results reported in Figure 10 of [23]. The ratio $R_{21} = {}^{65}T_1^{-1}/{}^{63}T_1^{-1}$ is also shown. It can be compared with $({}^{65}{\rm Q}/{}^{63}{\rm Q})^2 = 0.85$ that would indicate fluctuating electric field gradients as main relaxation mechanism, $({}^{65}\gamma/{}^{63}\gamma)^2 = 1.15$ indicating electron-spin nuclear-spin magnetic hyperfine interaction and $({}^{65}\gamma/\,{}^{63}\gamma)^4 = 1.32$ yielding the limiting value of direct or indirect nuclear-spin nuclear-spin contributions. The predominance of electron-spin nuclear-spin coupling is supported. The corresponding Korringa-like slopes (r_1) are collected in Table 5. The slopes derived from $1/T_1$ and $1/T_2$, respectively, for the $\underline{\rm E}_z$-lines are rather similar, whereas those for the $\underline{\rm C}_z/\underline{\rm D}_z$- and $\rm C_z/D_z$-lines differ by a factor of two. This reflects that only the $+1/2 \leftrightarrow -1/2$ transitions are excited for the latters, whereas all transitions contribute for the $\underline{\rm E}_z$-lines, because the quadrupolar splitting for this $\underline{\rm E}_z$-line is smallest. Like for the $1/T_2$ rates, the extrapolated zero-temperature rates (r_0) of $1/T_1$ amount to 0.8 – 0.9 ms^{-1} for the $\underline{\rm E}_z$ lines, whereas those of the $\underline{\rm C}/\underline{\rm D}$ and C/D-lines are 0.2 – 0.3 ms^{-1} only. Due to the substantial paramagnetic line shifts, it was difficult to derive reliable relaxation data for individual quadrupole satellite lines. A comparatively larger T-independent contribution seemed to outweigh the Korringa-like increase of $1/{\rm T}_1$, however.

Table 5. Korringa-like slopes "r_1" of $+1/2 \leftrightarrow -1/2$ transition relaxation rates, units s^{-1}K^{-1}.

NMR-line	^{63}Cu		^{65}Cu	
	$(1/T_1)$	$(1/T_2)$	$(1/T_1)$	$(1/T_2)$
$\underline{\rm E}_z$	3.9	5.3	5.8	6.0
$\underline{\rm C}_z/\underline{\rm D}_z$, $(\cos^2\vartheta \approx 0)$	4.2	8.0	4.6	8.5
$\rm C_z/D_z$, and $\underline{\rm C}_z/\underline{\rm D}_z$, $(\cos^2\vartheta \approx 5/9)$	3.3	7.0	3.3	8.0

5 Discussion

The ^{63}Cu and ^{65}Cu nuclei are used here in order to probe the static and dynamic part of hyperfine interaction of the heavy-fermion paramagnet $CeCu_6$. In the high-temperature orthorhombic structure of this compound, five inequivalent Cu sites must be distinguished and six in the low-temperature monoclinic phase [9]. The Cu(3) site

is the Cu site with the largest distance to its three Ce nearest neighbours in $CeCu_5Au$ [11], *i.e.* $d = 3.263$ Å in the average. If the association of NQR-lines and Cu sites in [20] is correct, by observing only NMR signals corresponding to the Cu[I] NQR line, only this Cu(3) site was characterized in our earlier NMR analysis of $CeCu_5Au$. C/D NMR lines, corresponding to the NQR lines I (Tab. 1), were now also identified in $CeCu_6$. In contrast to the anisotropic heavy-fermion antiferromagnet $CeCu_5Au$ with a Néel temperature $T_N = 2.3$ K, in which the transferred field coupling constant α of this site amounts only to $+(1.21-1.26)\,\mathrm{kOe}/\mu_B$ [23], a considerably stronger average hyperfine interaction of $\alpha = (1.46-3.35)\,\mathrm{kOe}/\mu_B$ is derived for the heavy-fermion paramagnet $CeCu_6$ here. This increase parallels a reduction of the unit cell volume by 3.3% or of the nearest Ce neighbour separation by 0.8% [9,11]. It is in conflict with the underlying volume independence of the RKKY-function [7,8] and points to a more local, covalency and overlap mediated mechanism of exchange and transferred hyperfine interaction in these intermetallic compounds.

No relevant difference of the main values of the quadrupolar splitting frequencies of $CeCu_5Au$ and $CeCu_6$ is observed for the Cu[I] line (Tab. 3, and Tab. 2 of [23]). The central NMR lines C_z/D_z and $\underline{C}_z/\underline{D}_z$, that show an orientation average of relaxation rates for this site, exhibit Korringa-like contributions to the $1/T_2$ and $1/T_1$ relaxation rates of $CeCu_6$. This is quite different from the a-direction of $CeCu_5Au$, where overall larger rates, with temperature independence of $1/T_2$ for temperatures above 20 K, and a $1/T_1$ rate increasing for decreasing temperature, were observed. This indicates clear differences of the spin dynamics of the para- and antiferromagnetic compounds. The Korringa-like temperature dependent increase of $1/T_1$ and $1/T_2$ for the C/D-lines, given in Table 5, is larger than the contribution of $(0.6-2.3)\,\mathrm{s^{-1}K^{-1}}$ or $(0.7-2.7)\,\mathrm{s^{-1}K^{-1}}$, estimated on the premises of purely *s*-like conduction electrons from the extrapolated Knight shift $K_0 = (0.15-0.29)\%$ (Fig. 4) with the familiar Korringa relation [27] for ^{63}Cu or ^{65}Cu, respectively. Increased relaxation rate for decreased Knight shift is the well-known consequence of superimposed 4*s*-like and 4*p*-like conduction electron contributions at Cu sites [8], however. (For Cu, hyperfine fields of +2.7 MOe per 4*s* electron spin, and −0.27 MOe per 4*p* electron spin, have to be considered [8].) The presence of *p*-like contributions for the Cu[I] line, or at the Cu(3) site, was evident already from anisotropy of the Knight shift of this site in $CeCu_5Au$ [31]: $K_{0,c} = +0.34\%$, but $K_{0,a} = +0.21\%$, were observed there. In summary, the Cu[I] NQR line is observed here as the C/D NMR lines of $CeCu_6$ and was identified with similar ν_Q-parameters in $CeCu_5Au$. This Cu site shows the smallest, positive transferred field coupling constant α of all observed Cu sites. This would be an argument in favour of associating these signals with the Cu(3) site, as was suggested in [20], because this is the site with the largest average separation from its three nearest Ce neighbours. This assignment conflicts with the rather large dipolar field anisotropy predicted for this site, in contrast to the negligible anisotropy observed in $CeCu_5Au$, however.

The other extreme of the transferred field coupling strength is found for the central $\underline{E}_z$ lines of $CeCu_6$ (Figs. 2 and 3). According to the Jaccarino-Clogston plot in Figure 4, these lines are observed only for magnetic field along the crystallographic a direction. If the assignment of NQR-lines and Cu sites of [20] is correct, the E-lines, exhibiting negligible quadrupolar splitting (Cu[0] in Tab. 1), originate from the Cu(5) sites. The Cu(5) site has the shortest separation from its three Ce^{3+} neighbours, $\bar{d} = 2.948$ Å [9], that is about 9% closer than the Cu(3) site. It is most important to point to the opposite sign and substantially increased strength of the transferred hyperfine coupling of this line or to this Cu site (Tab. 4). This large coupling constant can explain, that the NMR signals corresponding to the *c* direction, that gives rise to a much larger magnetic susceptibility, are shifted and broadened so severely that they are unobserved for our polycrystalline powder sample. The Korringa-like part of the $1/T_2$ and $1/T_1$ relaxation rates of these lines is, evidently, not increased in proportion to α^2, pointing to the difference of static and dynamic contributions of the transferred hyperfine interaction (compare Tabs. 4 and 5). However, a comparatively larger importance of *s*-like conduction electrons for this site is deduced from the larger extrapolated Knight shift of $K_0(\underline{E}) = +0.32\%$ (Fig. 4). The Korringa relation [27] predicts then relaxation rates of 2.8 $\mathrm{s^{-1}K^{-1}}$ (3.2 $\mathrm{s^{-1}K^{-1}}$) for ^{63}Cu (^{65}Cu), already within a factor of two to experimental observation (Tab. 5).

The large differences of the coupling constants α collected in Table 4 must be confronted with the prediction of the RKKY model [7,8].

$$\alpha_{i(\mathrm{Cu})}^{\mathrm{RKKY}} = -\frac{6(g_J-1)\pi}{g_J\mu_B^2} z K_0 J(0) \sum_{j(\mathrm{Ce})} F(2k_F r_{ij}) \qquad (3)$$

with the RKKY function

$$F(2k_F r) = \left[(2k_F r)\cos(2k_F r) - \sin(2k_F r)\right]/(2k_F r)^4 \qquad (4)$$

and the Fermi wave number

$$k_F = (3\pi^2 Z_{u.c.}/V_{u.c.})^{1/3} \qquad (5)$$

amounting to about 1.3634 $\mathrm{Å^{-1}}$ for $CeCu_6$. Here $z = 1.286$, $Z_{u.c.} = 36$ is the average number of conduction electrons per atom or unit cell of volume $V_{u.c.}$ (4 formula units), respectively, $J(0)$ the exchange integral, $g_J = 6/7$ for Ce^{3+} and the summation in equation (3) runs for the respective Cu site i over all Ce sites *j*. These values are tabulated in Table 1 in relative units, reporting only the results of the RKKY-sum of equation (3) ($r_{ij}(\max) = 800$ Å). Evidently, the RKKY-sum by itself can not explain a change in sign of the coupling constant α (Tabs. 1 and 4)!

In order to allow an estimate of the relative importance of classical dipolar contributions to the coupling constant α (Eq. (1)), respective calculated values for Ce-moments along *a*, *b* or *c* direction are included in Table 1. It is selfexplanatory that the classical dipolar field can not at all explain the change in sign of the coupling constants α observed.

It is thus evident, that the simplified RKKY-model (Eq. (3)) can not explain the differences of the observed coupling constants. It gives nevertheless reasonable order of magnitude estimates. *E.g.* for the Cu(3) site, with $K_0 = 0.22\%$ (Fig. 4), we derive $J(0) = -0.38\,\mathrm{eV}$ from equation (3), in the typical order of magnitude of effective $4f$-spin s/p-conduction electron exchange in rare earth intermetallics [8]. For the E-lines, if originating from the Cu(5) sites, we estimate from $\alpha = -6.7\,\mathrm{kOe}/\mu_B$, $K_0(\mathrm{E}) = +0.32\%$ and $\sum F(2k_F r) = -2.4 \times 10^{-3}$ an effective $4f$-spin s/p-conduction electron exchange integral of $J(0) = +1.2\,\mathrm{eV}$, *i.e.* of comparable absolute value, but opposite, *i.e.* ferromagnetic sign. The RKKY model predicts also the asymptotic Curie temperature (for the high-temperature limit of isotropic Ce moments) [7,8]. With $\sum F(2k_F r) = -1.18 \times 10^{-3}$ for the Ce site, we calculate $\theta_p = +0.12\,\mathrm{K}$ $(+1.9\,\mathrm{K})$ for the two estimates of $J(0)$, thus again of a reasonable order of magnitude.

The different signs and the sign conventions of the exchange parameter $J(0)$ require further discussion. Most generally, the hyperfine field at the non-magnetic s/p-metal partner site of rare earth intermetallic compounds is negative or antiparallel to the $4f$-spin moment [8]. This corresponds typically also to a negative, *i.e.* antiferromagnetic exchange parameter $J(0)$ in equation (3). Whereas Hund's rule intraatomic $4f$-$5d$ or $4f$-$6s/p$ exchange is allways ferromagnetic at the rare earth atom, hybridization of the latter electrons with the neighbour atom's outer electrons leads to the sign change of $J(0)$. The well-known consequence for the ${}^2F_{5/2}$ Hund's rule ground state of the light rare earth ion Ce^{3+} is that, because the small spin moment ($S = 1/2$) is oriented opposite to the large orbital moment ($L = 3$) (yielding the small Landé g-factor $g_J = 6/7$), the transferred hyperfine field at the "non-magnetic" neighbour is positive and parallel to the total rare earth electronic moment, as is reflected by the positive sign of the coupling constant α of the B, C and D sites (Tab. 4) – inspite of the negative $J(0)$. These considerations are described by the $(g_J - 1)$ proportionality in equation (3), and differ significantly from the proportionality of the classical dipolar field, *i.e.* α^{dip} in Table 1, to the total $4f$ electronic magnetic moment.

The positive, *i.e.* ferromagnetic, sign of $J(0)$, and the corresponding negative value of α for the E-lines (supposedly Cu(5) sites), that have an unusually small separation from the three neighbouring Ce^{3+} ions, points to predominance of direct admixture of the ferromagnetically polarized outer rare earth $5d$ and $6s/p$-orbitals into the "non-magnetic" Cu neighbour's $4s$-like wave functions. The negative sign of the coupling constant α is also clearly shown for the A-lines (Fig. 5 and Tab. 4) The change in sign is thus not the consequence of some RKKY-like spatially oscillating conduction electron polarization, but seems to be due to the short-range interaction resulting from the unusually small Ce-Cu separation of some sites in $CeCu_6$. Covalent bonding-like interactions must result for these partners in the intermetallic compound, a suggestion that might be verified by appropriate band-structure calculations for the heavy-fermion paramagnet $CeCu_6$. Due to the L minus S coupling of the Ce^{3+} ground state, this "ferromagnetic" Cu-neighbour $4s/p$ spin polarization actually is shielding the cerium $4f$ electronic moment antiferro- (or better ferri-) magnetically.

Before concluding, it is worth mentioning that the average value, over all orientations and Cu sites, of the transferred field coupling constant α is rather small, and positive: $\overline{\alpha} = +0.5\mathrm{kOe}/\mu_B$ can be calculated from early NMR analysis of $CeCu_6$ in the $140-470\,\mathrm{K}$ range [8], where $J_{sf} = -0.012\,\mathrm{eV}$ was derived in the frames of the uniform polarization model [32,33]. Thus it is important to remember for specific heat and other integral analyses of the heavy fermion compounds $CeCu_{6-x}Au_x$, that the internal fields are more than one order of magnitude larger than their average value, because ferromagnetic and antiferromagnetic polarization mechanisms compete.

6 Concluding remarks

In summary, five different Cu sites have been detected in our NMR studies of (oriented) powder samples of the heavy-fermion paramagnet $CeCu_6$. Relaxation at the other sites must be too fast, and the strength as well as anisotropy of the transferred hyperfine interaction might be too pronounced to allow their measurement under our current experimental conditions. It seems important to remind, furthermore, that the comparison of our NMR spectroscopic and relaxation data with earlier published results reveals [19,21,22,29], that the spin dynamics of some of the Cu sites seemingly have not been studied at all, up to now. For at least two different Cu sites of the heavy fermion paramagnet $CeCu_6$, studied here, nuclear spin lattice relaxation at temperatures above 10 K seems primarily governed by the local conduction electron state density and their $4s$- or $4p$-like character. The influence of the dynamic part of the transferred hyperfine interaction for the Cu nuclear spin-lattice relaxation grows with the slowing-down of the $4f$ electron spin correlations for decreasing temperatures. Thus the respective contribution dominates for the Cu[I] lines in the heavy-fermion antiferromagnet $CeCu_5Au$ for magnetic field perpendicular to the magnetically "easy" c-axis already over the Korringa-like conduction electron contribution for temperatures ranging below 80 K [23], in contrast to the heavy-fermion paramagnet $CeCu_6$ studied here at $B_0 = 7\,\mathrm{T}$, where lower temperatures would be required to accentuate this contribution.

We have derived the coupling constants $\alpha_i(n)$ for the hyperfine field, transferred from the Ce-$4f$ moments to five different Cu sites in $CeCu_6$ for at least one direction of the magnetic field with respect to the crystallographic axes. These coupling strengths α_i are in part more than a factor of 10 larger than the average value $\overline{\alpha} = +0.5\,\mathrm{kOe}/\mu_B$ known from high-temperature NMR (140−470 K) [32,33]. Positive as well as negative coupling constants are observed, in contrast to the predictions of the simple RKKY model. The transferred fields are extremely anisotropic, yet less due to an anisotropy of the coupling constant α, but primarily due to the almost Ising-like anisotropy of the low-temperature cerium

moment. A strong volume dependence of the Ce to Cu transferred hyperfine interaction may be surmised for the Cu[I] sites by comparison of the NMR results for the coupling constant $\alpha[\mathrm{I}] = +1.21 - 1.26\,\mathrm{kOe}/\mu_B$ for $CeCu_5Au$ and $\alpha[\mathrm{I}] = +1.5 - 3.4\,\mathrm{kOe}/\mu_B$ for $CeCu_6$. We suggest that the competition between the ferro- and the antiferromagnetic Cu-4 s/p-like electron spin polarization might be the reason for the pronounced influence of the nominally isoelectronic – but volume-influential – substitution of Cu by Au in the heavy-fermion pseudobinary compounds $CeCu_{6-x}Au_x$.

The comparatively large local transferred fields at the Cu sites, that add up to a ten-times smaller average field due to the difference in sign, have to be kept in mind, if, *e.g.*, the ac-susceptibility in an oscillating field of 10 mOe amplitude is measured in the temperature range down to 250 μK [4]. Care is even more severely required, if effective Curie constants *via* $C^{-1} = \frac{\mathrm{d}}{\mathrm{d}T}\left[\left(\frac{\Delta M_{ac}}{H_{ac}}\right)^{-1}\right]$ are then extracted in $CeCu_6$, corresponding only to two to eight times the Cu nuclear moments' value [4]. The enhancement of external static or oscillating fields at the nuclear sites is, in principle, well known [8], and the distinction between electronic and nuclear ordering (or freezing) processes in the milli- to micro-Kelvin range of $CeCu_6$ is thus highly recommended.

In summary, we proved the competition of two polarization mechanisms in $CeCu_6$: Supposedly along the path of very short Ce-Cu-Ce separations, ferromagnetic polarization of the electron spins is transferred, and thus, due to the L minus S orientation in Ce^{3+}, ferrimagnetic orientation of the respective total local magnetic moments at the Ce and the Cu sites. This mechanism favours interaction along the b-direction and leads to partial shielding of the Ce^{3+} magnetic moment by Cu conduction electrons. The second contribution yields an antiferromagnetic spin coupling or antiferromagnetic effective exchange interaction, predominating at the more distant Cu neighbours of the Ce^{3+} ions. *Via* this sign of the coupling, the total magnetic moment is increased compared to the bare Ce^{3+} moment. Thus both mechanisms counteract, and according to the average high-temperature transferred hyperfine field at all Cu sites, the antiferromagnetic exchange path just barely wins in $CeCu_6$. The variation of these two contributions with x in $CeCu_{6-x}Au_x$, responsible for the transition from heavy-fermion paramagnet to antiferromagnet is an objective of future research. The coupling constants $\alpha_i(n)$ of the transferred fields at the Cu sites in $CeCu_6$ are anisotropic, but much less than the low-temperature local Ce^{3+} moments, that by superposition yield a magnetically "easy" c-axis, "hard" b-axis and "intermediate" a axis. It is necessary to emphasize that the interpretation of the NMR results presented here must be considered as tentative, because a polycrystalline powder sample with non-ideal field-orientation characteristics was used for the measurements. An even more detailed NMR analysis of a single crystal is required in order to assign unequivocally the various Cu sites to NMR lines, electric field gradients, conduction electron densities and spin polarizations, however.

We thank H.v. Löhneysen for stimulating these investigations. K.H. Diefenbach and O. Stockert prepared the powder sample, M.T. Kelemen performed the early susceptibility measurements. We are indepted to T. Wokrina for valuable assistance.

References

1. H.v. Löhneysen, J. Magn. Magn. Mater. **200**, 532 (1999).
2. Y. Onuki, T. Komatsubara, J. Magn. Magn. Mater. **63+64**, 281 (1987).
3. A. Amato, D. Jaccard, J. Flouquet, F. Lapierre, J. Tholence, R.A. Fisher, S.E. Lacy, J.A. Olsen, N.E. Phillips, J. Low Temp. Phys. **68**, 371 (1987).
4. H. Tsujii, E. Tanaka, Y. Ode, T. Katoh, T. Mamiya, S. Araki, R. Settai, Y. Onuki, Phys. Rev. Lett. **84**, 5407 (2000).
5. C. Paschke, C. Speck, G. Portisch, H.v. Löhneysen, J. Low Temp. Phys. **97**, 229 (1994).
6. H.v. Löhneysen, T. Pietrus, G. Portisch, H.G. Schlager, A. Schröder, M. Sieck, T. Trappmann, Phys. Rev. Lett. **72**, 3262 (1994).
7. K. Yosida, Phys. Rev. **106**, 893 (1957).
8. E. Dormann, *NMR in intermetallic compounds*, in: *Handbook on the physics and chemistry of rare earths*, edited by K.A. Geschneidner Jr., L. Eyring (Elsevier/ North-Holland, Amsterdam 1991), Vol. 14, Chap. 94, p. 63 and references therein.
9. D.T. Cromer, A.C. Larson, R.B. Roof Jr., Acta Cryst. **13**, 913 (1960).
10. M.L. Vrtis, J.D. Jorgensen, D.G. Hinks, Physica B **136**, 489 (1986).
11. M. Ruck, G. Portisch, H.G. Schlager, M. Sieck, H.v. Löhneysen, Acta Cryst. B **49**, 936 (1993) .
12. Bruker, *Almanach* (Rheinstetten/Karlsruhe, 1999).
13. D.R. Lide, *CRC Handbook of Chemistry and Physics*, 76th edn. (CRC Press, Inc., Boca Raton, Florida, 1995-96).
14. Y. Onuki, Y. Shimizu, T. Komatsubara, J. Phys. Soc. Jpn **54**, 304 (1985).
15. S. Zemirli, S. Barbara, Solid State Communic. **56**, 385 (1985).
16. S. Takayanagi, Y. Onuki, T. Komatsubara, J. Phys. Soc. Jpn **55**, 2384 (1986).
17. J. Rossat-Mignod, L.P. Regnault, J.L. Jacoud, C. Vetter, P. Lejay, J. Flouquet, E. Walker, D. Jaccard, A. Amato, J. Magn. Magn. Mater. **76+77**, 376 (1988).
18. B. Stroka, A. Schröder, T. Trappmann, H.v. Löhneysen, M. Loewenhaupt, A. Severing, Z. Phys. B. **90**, 155 (1993).
19. T. Shimizu, M. Takigawa, H. Yasuoka, Y. Onuki, T. Komatsubara, J. Phys. Soc. Jpn **54**, 470 (1985).
20. K. Kumagai, I. Watanabe, H. Nakajima, Y. Onuki, T. Komatsubara, Jpn J. Appl. Phys. **26**, Suppl. 26-3, 533 (1987).
21. Y. Kitaoka, K. Fujiwara, Y. Kohori, K. Asayama, Y. Onuki, T. Komatsubara, J. Phys. Soc. Jpn **54**, 3686 (1985).
22. K. Kumagai, H. Aoki, H. Nakajima, Y. Onuki, T. Komatsubara, Jpn J. Appl. Phys. **26**, Suppl. 26-3, 531 (1987).
23. E. Kerscher, M.T. Kelemen, K.H. Diefenbach, O. Stockert, H.v. Löhneysen, E. Dormann, Eur. Phys. J. B **19**, 241 (2001).

24. The coupling constants reported in [23] had to be corrected due to a confusion of the susceptibility of $CeCu_5Au$ and $CeCu_{5.9}Au_{0.1}$ in Figure 2 of [23].
25. K.H. Diefenbach, Diplomarbeit, Universität Karlsruhe (1998), unpublished.
26. M. Winkelmann Diplomarbeit, Universität Karlsruhe (2001), unpublished.
27. A. Abragam, *The principles of nuclear magnetism* (Clarendon Press, Oxford, 1973).
28. G.C. Carter, L.H. Bennett, D.J. Kahan, *Metal shifts in NMR*, in: Progress in Material Science, Vol. 20, edited by B. Chalmers, J.W. Christian, T.B. Massalski (Pergamon Press 1977).
29. L. Pollack, J.R. Hoch, C. Jin, E.N. Smith, J.M. Parpia, D.L. Hawthorne, D.E. Geller, D.M. Lee, R.C. Richardson, D.G. Hinks, E. Bucher, Phys. Rev. B **52**, R 15707 (1995).
30. S. Koritnig, *Ionen- und Atomradien in Kristallen.* in: Landolt-Börnstein, Zahlenwerte und Funktionen, Bd. I/4, edited by K.H. Hellwege (Springer-Berlin 1955), p. 529.
31. E. Kerscher, Diplomarbeit, Universität Karlsruhe (2000), unpublished.
32. I. Pop, M. Coldea, V. Niculescu, Czech. J. Phys. B **24**, 1398 (1974).
33. M. Coldea, I. Pop, Acta Phys. Pol. A **48**, 359 (1975).